Thin Solid Films 745 (2022) 139096

Contents lists available at ScienceDirect

Thin Solid Films

journal homepage: www.elsevier.com/locate/tsf

Inkjet-printed indium sulfide buffer layer for Cu(In,Ga)(S,Se)$_2$ thin film solar cells

Alice Debot [a,*], Van Ben Chu [a], Damilola Adeleye [a], Jérôme Guillot [b], Didier Arl [b], Michele Melchiorre [a], Phillip J. Dale [a]

[a] Department of Physics and Materials Science, University of Luxembourg, 41 rue du Brill, Belvaux L-4422, Luxembourg
[b] Materials Research and Technology Department, Luxembourg Institute of Science and Technology, 41 rue du Brill, Belvaux L-4422, Luxembourg

ARTICLE INFO

Keywords:
Inkjet printing
Indium sulfide
Buffer layer
Aqueous solution
Ultra-violet ozone
Copper indium gallium selenide
Thin film solar cell

ABSTRACT

We report an environmentally friendly inkjet-printed indium sulfide (In_2S_3) buffer layer using benign chemistry and processing conditions. A pre-synthesized indium-thiourea compound is dissolved in a mixture of water and ethanol, inkjet printed on a Cu(In,Ga)(S,Se)$_2$ absorber and annealed in air. The buffer layer shows a β-In_2S_3 structure with few organic impurities and band gap in the range of 2.3 eV. An ultraviolet ozone treatment applied to the surface of the absorber prior to inkjet printing of the precursor is used to improve the wettability of the ink and therefore the surface coverage of the buffer on the absorber layer. The device with a fully covering In_2S_3 layer shows better open circuit voltage and fill factor than the device with a partially covering In_2S_3 layer. The best In_2S_3 device showed a light to electric power conversion efficiency similar to the reference cadmium sulfide buffer layer device. Good wettability conditions are therefore essential for higher efficiency solar cells when the buffer layer is inkjet-printed.

1. Introduction

Buffer layers are essential in thin film solar cells to help form the pn junction and ensure good band alignment between the absorber and the window layers. Cadmium sulfide (CdS) with a band gap of 2.4 eV is the most commonly reported buffer layer material in the literature for Cu(In,Ga)Se$_2$ (CIGSe) [1], CdTe [2] and kesterite [3] technologies. For CIGSe devices containing a CdS buffer layer, the highest reported light to electric power conversion efficiency (PCE) was 22.6% [4]. However, CdS is toxic and more environmentally friendly alternative compounds have attracted interest. One substitute is indium sulfide (In_2S_3) which is n-type doped with a reported band gap range between 2.01 eV [5] to 3.25 eV [6] with a consensus on the region between 2.1–2.5 eV. The wide range of reported values for the band gap is perhaps due to the different deposition techniques used to fabricate the buffer layer, the final compound stoichiometry and any remaining chemical impurities. Various device studies compared the efficiency of their In_2S_3 containing device with a reference CdS device. Ratios of In_2S_3 devices power conversion efficiency (PCE_{In}) to CdS devices efficiency (PCE_{Cd}) showed that In_2S_3 is a good candidate to replace the CdS, independent of the deposition technique, for example: physical vapor deposition (PVD) ($\frac{PCE_{In}}{PCE_{Cd}}$ = 1.07) [7], chemical bath deposition (CBD) (1.12) [8], atomic layer deposition (ALD) (1.20, 1.00) [9,10], spin coating (1.02) [11], spray pyrolysis deposition (1.36) [12]. It is also worth to mention the CBD deposited Zn-based buffer layer which led to the present record Cu(In,Ga)(S,Se)$_2$ (CIGSSe) device. The PCE ratio of Zn-based (PCE_{Zn}) device to CdS device is 1.02 [13]. However, all of the aforementioned deposition methods deposit material also in the sample surroundings, which reduces the material utilization.

Inkjet printing has recently gained interest as a deposition method of buffers such as Zn-based ($\frac{PCE_{Zn}}{PCE_{Cd}}$ = 1.18) [14] as well as absorber layers [15,16] because of its patterning flexibility and 100% material utilization. Wang et al. [11]. inkjet-printed an indium sulfide buffer layer on a CIGSe thin film. The ink was formulated by dissolving indium nitrate and thiourea (as a source of sulfur) in alcohol-based solution. The In_2S_3 buffer samples were dried at 150 °C in air and post annealed at 225 °C in H_2S. A slightly lower efficiency was found for the device with an In_2S_3 buffer compared to the CdS device ($\frac{PCE_{In}}{PCE_{Cd}}$ = 0.98). The In_2S_3 device showed an improved fill factor but a decreased open circuit voltage and short circuit current density compared to the CdS device.

In this work, we study the inkjet printing and annealing of In_2S_3 fabricated from an ink containing an indium-thiourea complex [17]. The

* Corresponding author.
E-mail address: alice.debot@uni.lu (A. Debot).

https://doi.org/10.1016/j.tsf.2022.139096
Received 18 June 2021; Received in revised form 17 December 2021; Accepted 12 January 2022
Available online 14 January 2022

pre-formed In-S bonds allow us to anneal our samples in air and therefore avoid the post annealing in toxic H_2S. Moreover, we study the effect of an ultraviolet (UV) ozone treatment to the surface of the absorber prior to the inkjet printing of the buffer layer in order to increase the wetting of the ink and ensure a complete coverage by the buffer layer. UV ozone is well studied because of its known capability to increase the wettability of materials. This techniques can clean surfaces of their organic contamination [18,19]. This treatment is also applied on polymeric substrates to improve the wettability (decreased contact angle) and adhesion [20]. We first analyze the crystallographic, morphological and optical properties as well as the chemical composition of an In_2S_3 layer. Then, we show the opto-electronic results of devices with a partially covering and fully covering In_2S_3 buffer. These surface coverages were varied by applying different UV ozone treatment times to the surface of the absorber.

2. Experimental details

2.1. Indium sulfide precursor and ink synthesis

Indium sulfide precursor was synthesized similarly to [17]. 16 g (0.21 mol) of thiourea (Alfa Aesar, ACS, 99% min) were dissolved in 100 mL of water under stirring. 14 g (0.063 mol) of anhydrous indium (III) chloride (Alfa Aesar, anhydrous, 99.999% (metals basis)) were added to the solution. When the solution became clear, it was heated to 80 °C until the appearance of tristhioureaindium(III) chloride ($In(TU)_3Cl_3$) as a white precipitate. The latter was filtered and washed with acetone and kept under vacuum.

The $In(TU)_3Cl_3$ was dissolved in a 3:1 water:ethanol solution with a total concentration of 0.8 mol/L to make an ink. The latter was filtered with a 0.2 μm pore filter (Whatman, PFTE) and injected in a 1 pL Dimatix cartridge.

2.2. Solar cell processing

The absorber was a 2 μm thick industrial CIGSSe layer. It was sputtered on 500 nm Mo-coated glass substrate. It was then annealed in sulfur and selenium containing atmosphere. Energy dispersive x-ray spectroscopy showed the absorber layer to have [Cu]/([Ga] + [In]), [Ga]/([Ga] + [In]) and [S]/([S] + [Se]) ratios of around 1.02 ± 0.12, 0.08 ± 0.05 and 0.10 ± 0.02, respectively. An approximate band gap of 1 eV was found by taking the maximum of the first derivative of the external quantum efficiency (EQE) as function of photon energy (dEQE/dE). All absorber layers used in the following study are from the same batch. The CIGSSe layers were etched with a 5% potassium cyanide solution for 30 s and dried with nitrogen. Then, a UV ozone treatment (Ossila, UV ozone cleaner) was applied to the absorbers prior to the deposition of the buffer precursor ink. The solution was inkjet printed (Fujifilm Dimatix DMP 2850) with a drop spacing of 35 μm. The voltages applied to the piezoelectric membranes were adjusted to have a stable printing. Since the ink had a low viscosity (0.9 mPa.s), the stability of the printing highly relied on the state of the nozzles. First time used nozzles ejected drops more steadily than already used nozzles. Voltage adjustment was thus a case-by-case optimization process. After the inkjet printing, the samples were annealed on a hot plate in air at 250 °C for 5 min. Finally, 50 nm intrinsic ZnO and 400 nm Al-doped ZnO window layers were sputtered at room temperature, followed by electron beam evaporation of the Ni/Al top contacts. The one square inch devices were manually scribed into cells with an area of 0.3 cm^2.

2.3. Characterization techniques

The structural properties of the In_2S_3 layers were analyzed by grazing incidence X-ray diffraction (XRD) (Bruker D8 Discover V2 with a Cu K_α radiation) with an incident angle of 0.5°. The chemical composition of the indium sulfide film was measured with energy dispersive X-ray spectroscopy (EDS) (Oxford, Aztec) at an accelerating voltage of 20 kV and a current of 1 nA and X-ray photoelectron spectroscopy (XPS) (Axis Ultra DLD) with a monochromated Al K_α X-ray source working at 225 W. The films were sputtered with Ar+ ions at 4 kV and 100 μA. The analyzed area had a diameter of 110 μm. The composition was extracted from EDS measurements using pre-measured standards. The [S]/[In] ratio was determined through EDS measurements on In_2S_3 deposited on glass, while XPS measurements revealed the residue content and the [S]/[In] in a film deposited on Mo coated glass. The optical properties (reflection and transmission) were studied with a UV Visible spectrometer (LAMBDA 950) with an integrating sphere and a home-built system for photoluminescence (PL) system with an excitation laser wavelength of 405 nm. From the transmission / reflection measurements, the direct band gap was extracted with a Tauc plot for direct allowed transition semiconductors: $(\alpha h\upsilon)^2 = C\,(h\upsilon - E_g)$ where E_g is the band gap, h is the Planck constant, υ the frequency of the photon, C is a constant and α is the absorption coefficient. The latter was determined by $\alpha = 2.303^*A/t$ where A is the absorbance and t the thickness of the film. The absorbance was calculated with the assumption that $A + T + R = 1$ where T is the transmittance and R the reflectance. The indirect band was extracted with a Tauc plot for indirect allowed transition semiconductors: $(\alpha h\upsilon)^{1/2} = C\,(h\upsilon - E_g)$. The surface morphology of the buffer layers was characterized by scanning electron microscopy (Zeiss SEM EVO10). A low accelerating voltage of 1 kV and a current of 500 pA were selected to study the morphology of the buffer layer deposited on the absorber, while an accelerating voltage of 10 kV and a current of 500 pA were used for higher magnification image of the absorber. The surface coverage of the buffer layer on the absorber was determined by analyzing SEM images at low accelerating voltage in ImageJ. The cross section imaging was performed with a focus ion beam scanning electron microscopy (FIB-SEM) (FEI Helios Nanolab 650) in secondary electron mode, using a 2 kV accelerating voltage. Prior to the FIB-SEM measurement, the samples were coated with a 30 nm Platinum protective layer by *ex-situ* sputtering (Leica ACE 600) and the cross-section zone was subsequently coated with a 1 μm *in-situ* Platinum layer by Ion Beam Induced Deposition using the Gallium source of the FIB-SEM instrument operating at 30 kV and 2 nA. The current - voltage characteristics were measured with an AAA solar simulator under 1 sun illumination conditions. EQE spectra were measured with a home-built system calibrated with Si and InGaAs references.

3. Results and discussion

In this section, we will first discuss the results of the characterization of the indium sulfide films deposited on glass and then discuss the opto-electronic properties of the devices.

3.1. Structural investigations

An X-ray diffractogram of an In_2S_3 thin film deposited on glass and annealed at 250 °C is presented in Fig. 1 and could be indexed to the β-In_2S_3 structure with a tetragonal crystal system. In this system, the angles of the unit cell are equal to 90° and the lengths of two edges (a and b) are equal. Our sample shows slightly shorter a and c edges than the reference structure. The calculated unit cell volume is 1843 $Å^3$, which is in accordance with the reference giving a volume of 1876 $Å^3$. The coherence length calculated on the Gaussian fitted (103) peak, using the Scherrer equation with a shape factor of 0.9, is 10 nm, which is roughly the grain size if we neglect the influence of stress in the film and suppose that the grains are spherical.

3.2. Chemical composition investigation

XPS and EDS measurements revealed the chemical composition of the indium sulfide film as described in Table 1. The [S]/[In] ratio was measured with EDS and XPS because of a possible preferential sputtering

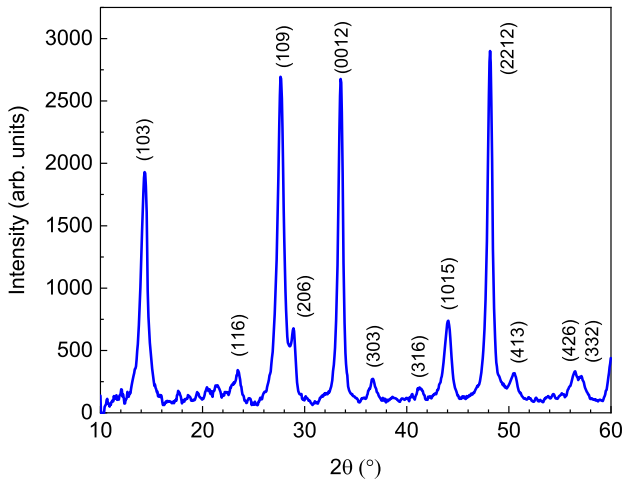

Fig. 1. Grazing incidence XRD of a β-In_2S_3 obtained from the annealing at 250 °C for 5 min of a precursor film deposited on glass. The peaks were identified with the reference PDF4+ 00-025-0390.

Table 1
Bulk chemical composition of an air annealed In_2S_3 film. The [S]/[In] ratio was measured with XPS and EDS, while the residues (O, N, Cl and C) were measured with XPS.

	[S]/[In] (EDS)	[S]/[In] (XPS)	[O] (at. %)	[N] (at. %)	[Cl] (at. %)	[C] (at. %)
Expected	1.5	1.5	0	0	0	0
Measured	1.4 ± 0.2	1.3 ± 0.1	0.5 ± 1.0	3.3 ± 1.0	3.5 ± 1.0	0

of the sulfur as already shown by Baker et al. for MoS_2 [21]. The ratio of [S]/[In] is 1.4 ± 0.2 according to EDS, which within the error gives the expected ratio for an In_2S_3 of 1.5. The oxygen content is found to be within the error of the measurement, proving the working principle of the indium-thiourea compound that the pre-formed In-S bond prevents indium oxide formation upon annealing in air. Residual nitrogen and chlorine were also found in the film each below 4 at.%. Carbon residue was only found on the surface and attributed to contamination from the environment.

3.3. Optical investigation

In order to determine the band gap, the precursor ink was drop casted on glass to form a 1.5 μm thick fully covering film. A room temperature PL spectrum (Fig. 2a) shows a broad peak centered around 2.3 eV, which appears to be the band gap. The width of this peak suggests that the In_2S_3 is rather defective or inhomogeneous. This value is in agreement with the band gap extracted from the EQE in the work of Wang et al. [11] (around 2.3 eV). The latter band gap was determined by digitizing the provided EQE and calculating the local maximum of the first derivative of the EQE as function of photon energy (dEQE/dE) in the expected energy range for the band gap. The direct or indirect nature of the band gap has already been discussed in literature without agreement. Zhao et al. [22] found with density functional theory that In_2S_3 has an indirect band gap of 2.07 eV. However, this band gap could also be defined as direct. Indeed, the energy difference between the highest valence band maximum (VBM) and the second highest VBM was found to be as small as 0.09 eV. Thus, the band gap determined with the second highest VBM and the conduction band minimum is direct. Barreau et al. [5] made a similar observation regarding the direct and indirect behavior using numerical approach. However, in these simulations, the In_2S_3 was supposed to be perfectly stoichiometric, which may not be true for our solution processed samples. In this work, the Tauc plot for a direct (indirect) band gap semiconductor (Fig. 2b) points to a band gap of 2.5 eV (2.1 eV) with a direct (indirect) allowed transition. The direct band gap of our In_2S_3 is thus similar to the band gap of CdS (2.4 eV) and is therefore a suitable candidate as a buffer layer to replace the CdS.

3.4. Ink coverage investigation

To investigate the role of UV-ozone exposure time on the wettability of the substrate by the precursor ink, the ink was printed on the CIGSSe absorber with a fixed drop spacing (35 μm) and the coverage was examined. In an ideal case, the neighbouring drops on the substrate should overlap with each other and form a continuous film. First, the precursor ink was deposited on a non-treated absorber. The surface of the CIGSSe was found to be highly hydrophobic. The dried drops diameters were on average 21 μm, which is insufficient to ensure an overlapping of the neighbouring drops as seen in Fig. 3(a). The total coverage of the absorber by the buffer layer was only 37%. In order to increase the hydrophilicity of the absorber, a UV ozone treatment was applied to the CIGSSe surface for 30 s prior to the inkjet printing. The wettability of the surface was improved, leading to an average droplet diameter of around 25 μm and a surface coverage of 53% (Fig. 3(b)). To obtain a fully covering buffer layer, 120 s UV ozone treatment was performed. After the inkjet printing, a continuous film was formed on the absorber thanks to the droplets diameter being 46 μm, enabling the overlapping of neighbouring drops (Fig. 3(c)). The succession of near vertical dark and lighter lines in the latter case is due to an imperfect

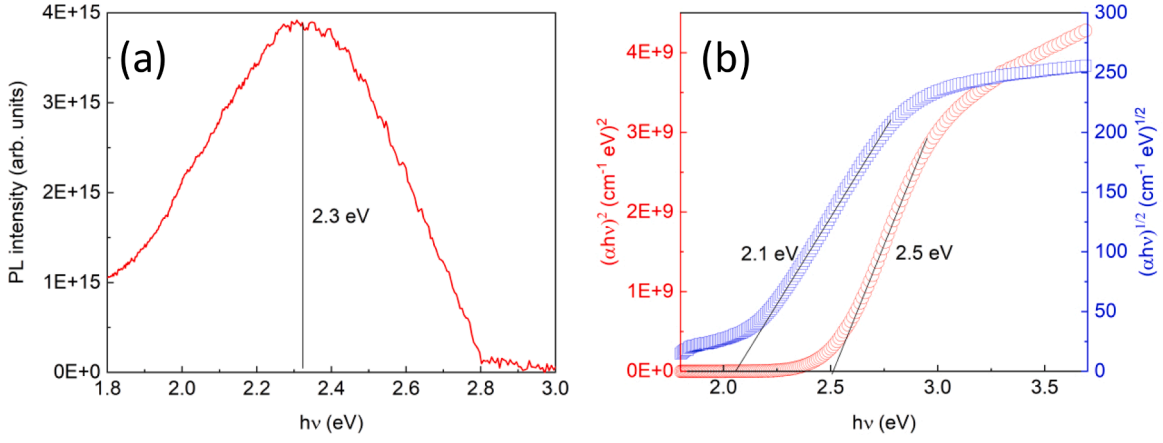

Fig. 2. PL measurement (a) and Tauc plot (b) for direct (red circle symbols) and indirect (blue square symbols) band gap semiconductor based on absorption data for In_2S_3 films on glass annealed at 250 °C in air.

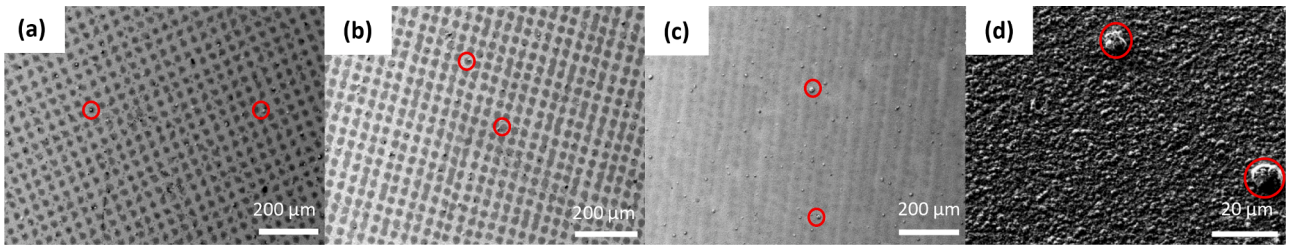

Fig. 3. Low magnification SEM top view images of annealed In_2S_3 layer deposited on CIGSSe absorber with (a) no UV ozone treatment, (b) 30 s of UV ozone and (c) 120 s of UV ozone on the surface of the absorber. (d) Higher magnification SEM top view image of bare CIGSSe. Red circles highlight small surface agglomerates on the surface of the samples that are attributed to the absorber.

overlapping of the neighbouring inkjet-printed lines, leading to an oscillation in the thickness of the film. The UV ozone treatment is thus found to be a critical parameter to ensure a continuous coverage of the buffer layer deposited on the absorber. A few scattered surface agglomerates that can be distinguished in the SEM images are related to the absorber and not the inkjet printing process since they are also observable in an SEM image of the bare absorber at high magnification (Fig. 3(d)).

In order to confirm the full coverage of the absorber by the buffer layer and to evaluate its morphology, a FIB-SEM image (Fig. 4) was taken for a 120 s UV ozone treated sample. The full device was first covered with 30 nm of Pt to protect the surface during the milling and to increase the conductivity, preventing charging of the specimen. The In_2S_3 buffer was found to fully cover the absorber surface, with a thickness varying from 80 to 120 nm. This variation is due to the high degree of roughness of the absorber: valleys were filled with more ink than the hills. Some voids appear in the layer which we speculate are due to bubbling during the annealing of the ink. The variation in buffer thickness may lead to detrimental electrical properties. Incidentally, some delamination of the absorber from the back contact (not shown here) were found, which would likely increase the series resistance of the device.

3.5. Device investigations

In this section, the effect of wetting and surface coverage on the current-voltage (JV) properties (Fig. 5) of the devices were studied. The partially covering (53%) and fully covering In_2S_3 are compared with a buffer free sample (represented by a 0% coverage) and a CdS reference already shown by some of the co-authors [14] since the same absorber material is used. The PCE of the CdS reference is relatively low compared to state of the art laboratory devices, but the absorber is reasonably uniform and efficient to allow us to elucidate the effect of the surface coverage. The best CdS reference device shows an efficiency of 11.4%, with an open circuit voltage (V_{oc}) of 536 mV, a short circuit current density (J_{sc}) of 38.1 mA/cm^2 and a fill factor (FF) of 56%. The best 100% covered In_2S_3 shows a slightly lower efficiency (10.9%) and J_{sc} (33.3 mA/cm^2) compared to the best reference device. In contrast, it shows an improved FF (58%) and V_{oc} (561 mV). Examining the literature, there is no clear trend regarding the difference of the In_2S_3 devices JV parameters compared to the CdS reference devices. The same trend as our work is observed for the CBD [8]. With PVD [7], the V_{oc} is improved but J_{sc} and FF are decreased, while in ALD [9] all the parameters were improved. In the inkjet-printing work of Wang et al. [11], the trend was partially similar to our work: the FF was improved and J_{sc} was decreased but the V_{oc} was also decreased.

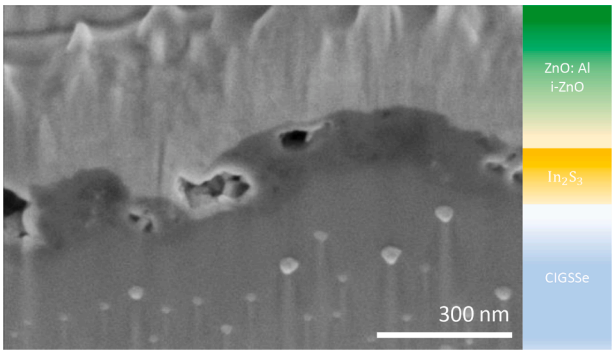

Fig. 4. FIB-SEM image of a 120 s UV ozone treated device with inkjet printed buffer layer and sputtered window layers. The white particles observed in the absorber layer are a redeposition effect inherent to gallium milling.

The PCE is found to increase with the surface coverage of the In_2S_3. The same trend as the efficiency is noticed in the open circuit voltage (V_{oc}), showing that V_{oc} increase is playing an important role in the efficiency improvement. The increase of the V_{oc} with the increase of the surface coverage may be reasonably explained by a decrease in sputter damage due to the deposition of the i-ZnO onto the absorber layer [23]. A different trend is observed for the J_{sc}: both In_2S_3 coverages exhibit a lower J_{sc} than buffer free and CdS samples with the highest surface coverage having the highest J_{sc}. To examine this trend further, EQE measurements were made of all the devices. Interestingly, the CdS device (Fig. 6) and the device without buffer layer show good collection at all wavelengths, corresponding to a higher J_{sc} (36.9 mA/cm^2 for buffer free, 38.1 mA/cm^2 for CdS). This indicates that the sputter damage is only sufficient to affect the voltage but not the current collection. The 53% and 100% covered In_2S_3 buffer layer devices have a lower collection over all wavelengths (33.3 mA/cm^2 for 100%, 32.0 mA/cm^2 for 53%). The typical "blue defect" absorption at short wavelengths is found for both CdS and In_2S_3 devices when compared with the buffer free device. The absorption at short wavelengths is different between the In_2S_3 samples because of the variation in their morphology. For the partially covering In_2S_3, the film is discontinuous, with thick droplet shape separated by buffer free space. On the opposite, the fully covering In_2S_3 is a continuous film but with a lower thickness. When comparing the 53% and 100% covered In_2S_3 buffer layer devices, it appears at longer wavelengths that the current collection is lower for the 53% coverage. Since the current collection of the 0% coverage is much higher in this region, we suppose that the collection length within the absorber is somewhat decreased, although the reason for this is unclear.

4. Conclusion

The use of a pre-synthesized indium-thiourea compound, $In(TU)_3Cl_3$, which was dissolved in a mixture of water and ethanol to make an ink, led to the formation of phase pure In_2S_3 upon annealing in air. The environmentally friendly characteristic of the In_2S_3 is thus preserved all along the process by suppressing the need for post annealing in H_2S. Films annealed in air showed a β-In_2S_3 structure, a low oxygen content and a band gap of around 2.3 eV, which is similar to the band gap of CdS. The surface coverage of the absorber by the buffer layer was varied by applying a UV ozone treatment to the CIGSSe surface prior to inkjet printing of the In_2S_3 precursor ink. A fully covering In_2S_3 led to a higher

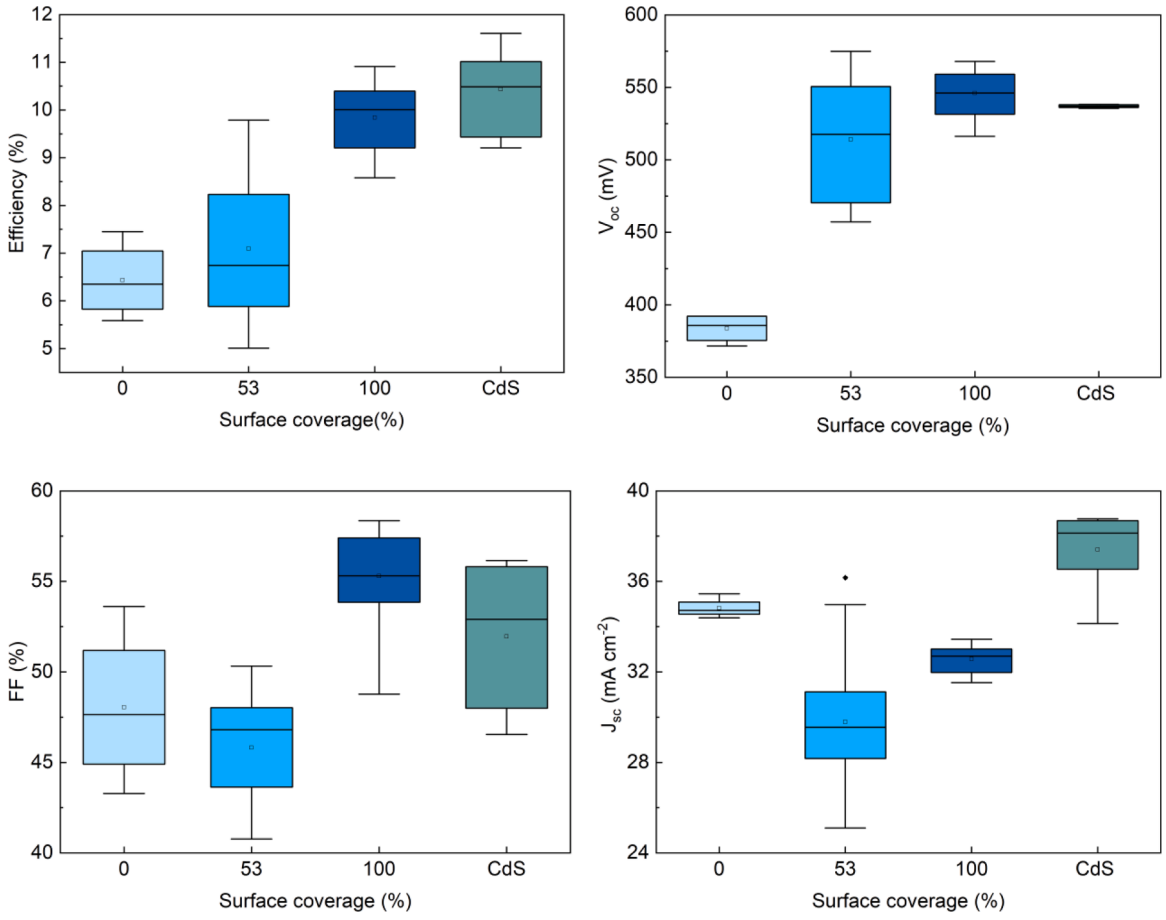

Fig. 5. Current-voltage characteristics of 16 cells: efficiency, open circuit voltage (V_{oc}), fill factor (FF), short circuit current density (J_{sc}). In blue, devices with an In_2S_3 buffer layer. In green, the reference devices with a CdS buffer layer.

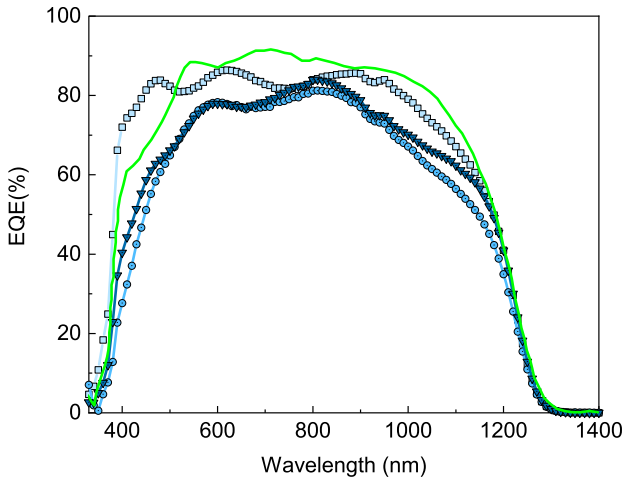

Fig. 6. EQE of CdS (solid line), buffer free (squares), In_2S_3 53% coverage (circles), In_2S_3 100% coverage (triangles) samples.

power conversion efficiency than the partially covering In_2S_3 mainly due to the improved open circuit voltage and fill factor. The best fully covering In_2S_3 was found to be nearly as good as the CdS, with a ratio $\frac{PCE_{In}}{PCE_{Cd}}$ of 0.92. A fully environmentally friendly and waste free buffer layer with similar efficiency than CdS seems to be a promising way through towards less toxic solar cells. Further studies on the annealing temperature and atmosphere of the ink are required in order to try to remove the remaining organic impurities whilst avoiding the formation of oxides in the buffer or destroying the delicate absorber-buffer interface. Additionally, to boost the short circuit current we aim to investigate how to minimize the parasitic absorption in the blue part of the spectrum by either reducing the thickness of the buffer layer or by increasing its band gap.

CRediT authorship contribution statement

Alice Debot: Conceptualization, Methodology, Validation, Investigation, Writing – original draft, Writing – review & editing, Visualization. **Van Ben Chu:** Investigation, Writing – review & editing. **Damilola Adeleye:** Investigation, Writing – review & editing. **Jérôme Guillot:** Investigation, Writing – review & editing. **Didier Arl:** Investigation. **Michele Melchiorre:** Investigation, Writing – review & editing. **Phillip J. Dale:** Conceptualization, Resources, Writing – review & editing, Supervision, Funding acquisition.

Declaration of Competing Interest

The authors declare no competing financial interest.

Acknowledgements

This work was supported by Fond National de la Recherche of Luxembourg through the STARSOL (C18/MS/12686759) and MASSENA (PRIDE15/10935404) projects. Susanne Siebentritt is acknowledged for helpful discussions. Brahime El Adib is acknowledged for depositing the Platinum.

References

[1] A. Kylner, Effect of impurities in the CdS buffer layer on the performance of the Cu(In, Ga)Se_2 thin film solar cell, J. Appl. Phys. 85 (1999) 6858, https://doi.org/10.1063/1.370204.

[2] A. Morales-Acevedo, Thin film CdS/CdTe solar cells: research perspectives, Sol. Energy. 80 (2006) 675–681, https://doi.org/10.1016/j.solener.2005.10.008.

[3] C.W. Hong, S.W. Shin, M.P. Suryawanshi, M.G. Gang, J. Heo, J.H. Kim, Chemically deposited CdS buffer/kesterite Cu_2ZnSnS_4 solar cells: relationship between CdS thickness and device performance, ACS Appl. Mater. Interfaces 9 (2017) 36733–36744, https://doi.org/10.1021/acsami.7b09266.

[4] P. Jackson, R. Wuerz, D. Hariskos, E. Lotter, W. Witte, M. Powalla, Effects of heavy alkali elements in Cu(In,Ga)Se_2 solar cells with efficiencies up to 22.6%, Phys. Status Solidi Rapid Res. Lett. 10 (2016) 583–586, https://doi.org/10.1002/pssr.201600199.

[5] N. Barreau, A. Mokrani, F. Couzinié-Devy, J. Kessler, Bandgap properties of the indium sulfide thin-films grown by co-evaporation, Thin Solid Films 517 (2009) 2316–2319, https://doi.org/10.1016/j.tsf.2008.11.001.

[6] E.B. Yousfi, T. Asikainen, V. Pietu, P. Cowache, M. Powalla, D. Lincot, Cadmium-free buffer layers deposited by atomic layer epitaxy for copper indium diselenide solar cells, Thin Solid Films 361 (2000) 183–186, https://doi.org/10.1016/S0040-6090(99)00860-3.

[7] P. Pistor, R. Caballero, D. Hariskos, V. Izquierdo-Roca, R. Wächter, S. Schorr, R. Klenk, Quality and stability of compound indium sulphide as source material for buffer layers in Cu(In,Ga)Se_2 solar cells, Sol. Energy Mater. Sol. Cells 93 (2009) 148–152, https://doi.org/10.1016/j.solmat.2008.09.015.

[8] D. Hariskos, M. Ruckh, U. Rühle, T. Walter, H.W. Schock, J. Hedström, L. Stolt, A novel cadmium free buffer layer for Cu(In,Ga)Se_2 based solar cells, Sol. Energy Mater. Sol. Cells 41–42 (1996) 345–353, https://doi.org/10.1016/0927-0248(96)80009-2.

[9] N. Naghavi, S. Spiering, M. Powalla, D. Lincot, Record efficiencies for dry processed cadmium free cigs solar cells with indium sulfide buffer layers prepared by Atomic Layer Deposition (ALD), in: Proceedings of the 3rd World Conference on Photovoltaic Energy Conversion, 2003, pp. 340–343, 10.1109/WCPEC.2003.1305289.

[10] D. Hariskos, S. Spiering, M. Powalla, Buffer layers in Cu(In,Ga)Se_2 solar cells and modules, Thin Solid Films 480–481 (2005) 99–109, https://doi.org/10.1016/j.tsf.2004.11.118.

[11] L. Wang, X. Lin, A. Ennaoui, C. Wolf, M.C. Lux-Steiner, R. Klenk, Solution-processed In_2S_3 buffer layer for chalcopyrite thin film solar cells, EPJ Photovolt. 7 (2016), https://doi.org/10.1051/epjpv/2016001.

[12] S.Y. Kim, M.S. Mina, K. Kim, J. Gwak, J.H. Kim, Application of a Sn4+ doped In_2S_3 thin film in a CIGS solar cell as a buffer layer, Sustain. Energy Fuels 4 (2019) 362–368, https://doi.org/10.1039/c9se00778d.

[13] M. Nakamura, K. Yamaguchi, Y. Kimoto, Y. Yasaki, T. Kato, H. Sugimoto, Cd-Free Cu(In,Ga)$(Se,S)_2$ thin-film solar cell with record efficiency of 23.35%, IEEE J. Photovolt. 9 (2019) 1863–1867, https://doi.org/10.1109/JPHOTOV.2019.2937218.

[14] V.Ben Chu, D. Siopa, A. Debot, D. Adeleye, M. Sood, A. Lomuscio, M. Melchiorre, J. Guillot, N. Valle, B. El Adib, J. Rommelfangen, P.J. Dale, Waste- and Cd-free inkjet-printed Zn(O,S) buffer for Cu(In,Ga)$(S,Se)_2$ thin-film solar cells, ACS Appl. Mater. Interfaces 13 (2021) 13009–13021, https://doi.org/10.1021/acsami.0c16860.

[15] X. Lin, R. Klenk, L. Wang, T. Köhler, J. Albert, S. Fiechter, A. Ennaoui, M.C. Lux-Steiner, 11.3% efficiency Cu(In,Ga)$(S,Se)_2$ thin film solar cells: via drop-on-demand inkjet printing, Energy Environ. Sci. 9 (2016) 2037–2043, https://doi.org/10.1039/c6ee00587j.

[16] W. Wang, Y.W. Su, C.H. Chang, Inkjet printed chalcopyrite CuInxGa1-xSe_2 thin film solar cells, Sol. Energy Mater. Sol. Cells 95 (2011) 2616–2620, https://doi.org/10.1016/j.solmat.2011.05.011.

[17] S. Wu, J. Jiang, S. Yu, Y. Gong, W. Yan, H. Xin, W. Huang, Nano energy over 12% efficient low-bandgap CuIn (S, Se) 2 solar cells with the absorber processed from aqueous metal complexes solution in air, Nano Energy 62 (2019) 818–822, https://doi.org/10.1016/j.nanoen.2019.06.010.

[18] J.R. Vig, UV/ozone cleaning of surfaces, Proc. Electrochem. Soc. 90 (1990) 105–113, https://doi.org/10.1116/1.573115.

[19] R. Kohli, UV-Ozone Cleaning for Removal of Surface Contaminants, Elsevier Inc., 2015, https://doi.org/10.1016/b978-0-323-29961-9.00002-8.

[20] M. Hamdi, J.A. Poulis, Effect of UV/ozone treatment on the wettability and adhesion of polymeric systems, J. Adhes. 97 (2021) 651–671, https://doi.org/10.1080/00218464.2019.1693372.

[21] M.A. Baker, R. Gilmore, C. Lenardi, W. Gissler, XPS investigation of preferential sputtering of S from MoS_2 and determination of MoSx stoichiometry from Mo and S peak positions, Appl. Surf. Sci. 150 (1999) 255–262, https://doi.org/10.1016/S0169-4332(99)00253-6.

[22] Z. Zhao, Y. Cao, J. Yi, X. He, C. Ma, J. Qiu, Band-edge electronic structure of β-In_2S_3: the role of s or p orbitals of atoms at different lattice positions, ChemPhysChem 13 (2012) 1551–1556, https://doi.org/10.1002/cphc.201100968.

[23] P. Soni, M. Raghuwanshi, R. Wuerz, B. Berghoff, J. Knoch, D. Raabe, O. Cojocaru-Mirédin, Sputtering as a viable route for In_2S_3 buffer layer deposition in high efficiency Cu(In,Ga)Se_2 solar cells, Energy Sci. Eng. 7 (2019) 478–487, https://doi.org/10.1002/ese3.295.